 doi:10.20944/preprints201706.0030.v1

Article

4SM: A Novel Self-calibrated Algebraic Ratio Method for Satellite Derived Bathymetry and Water Column Correction

Yann G. Morel *

* Correspondence: rspfsm@watercolumncorrection.com

Abstract: All empirical water column correction methods have consistently been reported to require existing depth sounding data for the purpose of calibrating a simple depth retrieval model; they yield poor results over very bright or very dark bottoms. In contrast, we set out to (i) use only the relative radiance data in the image along with published data, and several new assumptions, (ii) in order to specify and operate the simplified radiative transfer equation (RTE), (iii) for the purpose of retrieving both the satellite derived bathymetry (SDB) and the water column corrected spectral reflectance over shallow seabeds. Sea truth regressions show that SDB depths retrieved by the method only need tide correction. Therefore it shall be demonstrated that, under such new assumptions, there is no need (i) for formal atmospheric correction, (ii) nor for conversion of relative radiance into calibrated reflectance , (iii) nor for existing depth sounding data, to specify the simplified RTE and produce both SDB and spectral water column corrected radiance ready for bottom typing. Moreover, the use of the panchromatic band for that purpose is introduced. Altogether, we named this process the Self-Calibrated Supervised Spectral Shallow-sea Modeler (4SM). This approach requires a trained practitioner, though, to produce its results within hours of downloading the raw image. The ideal raw image should be a "near-nadir" view, exhibit homogeneous atmosphere and water column, include some coverage of optically deep waters and bare land, and lend itself to quality removal of haze, atmospheric adjacency effect, and sun/sky glint.

Keywords: remote sensing; attenuation coefficient; ratio method; soil line; bottom reflectance; shallow substrate; satellite derived bathymetry; water column correction; bottom typing

1. Introduction

Since the advent of LANDSAT MSS, most projects of passive remote sensing of SDB required the use of at least a few existing bottom depth points to derive empirical linear regressions between water depths and measured spectral radiance or reflectance at the base of the atmosphere. They use a simplistic statistical equation, assume homogeneous optical properties of the atmosphere and water column, and do not consider the optical properties of the water column.

Most empiric approaches only yield SDB [1,2], but they are fairly simple and fast to operate, and therefore widely used. Although they have been recently reported to be useful by the hydrographic community [3], and feature in the International Hydrographic Organisation's cookbook [4], and in a commercial package [5], they have long been known to yield biased results over highly reflecting seabeds at very shallow depths, and also over poorly reflective seabeds [6,7]**:** if at all possible, they need to be improved [8,9]. Besides, a simple operational work flow must be offered in order to process the recent abundance of freely available quality image data like LANDSAT-8.

In contrast, since the turn of the century, several analytical methods use a general optical equation dependent on intrinsic optical properties of sea water, illumination and viewing geometry, atmospheric and glint effects, *etc*. [10]. They require a look-up table (LUT) of spectral reflectance for all possible bottom substrates over the whole shallow depth range, for a wide range

of those many factors. Then for each shallow pixel, the correct depth is chosen through a computer-intensive spectral matching optimization technique, which also yields the water column corrected spectral bottom reflectance and the spatial variations of the optical properties of the water column. This approach has recently shown promise in the hands of several teams of advanced R&D scientists using a very complex work flow and powerful computing [11], and has even been implemented in a commercial software package [12].

In this paper, a well researched and accepted simplified RTE is summarized, and several new assumptions are introduced to operate it in a band combination approach. Then, the proposed work flow to derive both the SDB and and the water column corrected spectral reflectance of the shallow bottom ready for bottom typing is detailed and illustrated. This work flow does not require the conversion of the relative radiance data into calibrated reflectance, and, most importantly, does not require existing depth sounding data to calibrate the RTE. This was first presented in 1998 by Morel and Lindell [13], and used by Favoretto et al. [14]. The following paper draws on the 23 years long study, in quasi-isolation, of hundreds of multispectral and hyperspectral images, airborne and spaceborne, worldwide (aerial photography, LANDSAT, SPOT, QUICKBIRD, WORLDVIEW-2, Compact Airborne Spectrographic Imager (CASI), HYPERION, even Hyperspectral Imager for the Coastal Ocean (HICO)); it reflects the experience gained at sea level, but also at high altitude (melt water ponds in Greenland, briny shallow lakes in Altiplano), under clear skies, but also under overcast skies in the Middle East. It includes several time series of LANDSAT and WORLDVIEW-2 images, and covers from very high (1 m GSD) to very coarse spatial resolution (100 m GSD), as illustrated at http://www.watercolumncorrection.com.

For a recent and comprehensive introduction to the basics of water column correction, and to no less than eighteen methodological approaches, sorted into band combination, model-based algebraic, optimization/matching, and multi-temporal analysis categories, please refer to a review by Zoffoli et al. [15]. These authors view the simplified RTE approach as an algebraic model-based algorithm, and conclude: "*More complex algebraic algorithms have been developed to estimate the reflectance in shallow environments that require more field data. They are the only methods capable of estimating bottom reflectance. For this reason, improvements and validations of this group of algorithms should be encouraged.*" For more reviews, please see also Dekker et al. [11], and Carmody [8].

The purpose of this article is to demonstrate that there is no need for field data for the calibration of the simplified RTE, and that SDB is estimated as a by-product of the water column correction of the spectral bottom reflectance.

2. The simplified RTE

Preamble: as shall be exposed in section 2.2, inverting the model (3) in the model-based algebraic 4SM approach amounts to a simplistic spectral matching. Therefore it does not require L radiance terms to be converted into physical units of reflectance R: this is the advantage and privilege of a "ratio method", which is only concerned with ratios among numbers. Therefore also, in all that follows in this article, the terms reflectance or radiance or digital number (DN) are used interchangeably, meaning the relative intensity of the signal captured by the sensor.

2.1. An operational model

From albedo A and reflectances R, to radiances L or digital numbers, the reader is expected to have a fair understanding of the definitions and concepts in ocean color remote sensing. The spectral reflectance of shallow bottoms R or L, as measured at the base of the atmosphere (BOA), has suffered the diffuse attenuation of the solar light flux on its way down from sea-surface to bottom, then on its way up from bottom to sea-surface (1,2). This is described by the following simplified RTE, for Case-1 waters where the diffusion by mineral particles may be considered very

Preprints (www.preprints.org) | NOT PEER-REVIEWED | Posted: 6 June 2017 doi:10.20944/preprints201706.0030.v1

low. This RTE has been established and verified using irradiance measurements in water. Here it must be remembered that measuring the irradiance of the light flux, whether downward or upward, accounts for the fate of all photons in a hemisphere. In contrast, remote sensing devices collect photons through an extremely narrow field of view; this shall be discussed in section 6.3.

The simplified RTE was formulated by Philpot in 1989 [16], and by Maritorena et al. in 1994 [17]:

$$R = Rw + (A - Rw)/\exp(2K\Box Z) \quad . \qquad \text{BOA} \qquad (1)$$

It is rewritten it for BOA radiances L at the base of the atmosphere (this shall be discussed in section 6.3):

$$L = Lw + (LB - Lw)/\exp(2K\Box Z) \quad . \qquad \text{BOA} \qquad (2)$$

It is now inverted to yield the BOA water column corrected reflectance LB:

$$LB = Lw + (L - Lw)\Box\exp(2K\Box Z) \quad . \qquad \text{BOA} \qquad (3)$$

At the top of the atmosphere (TOA): add the atmospheric path radiance La to all L terms in (2):

$$L + La = Lw + La + (LB + La - Lw - La)/\exp(2K\Box Z) \quad . \qquad \text{TOA} \qquad (4)$$

So the simplified RTE at the top of the atmosphere becomes:

$$Ls = Lsw + (LsB - Lsw)/\exp(2K\Box Z) \quad . \qquad \text{TOA} \qquad (5)$$

Estimating the atmospheric path radiance in the absence of any glint:

$$La = Lsw - Lw \quad ; \qquad (6)$$

Estimating the BOA measured radiance in the absence of any glint:

$$L = Ls - La \quad . \qquad (7)$$

Linearizing the bottom contrast:

$$X = \log(Ls - Lsw) \quad . \qquad \text{Linearization} \qquad (8)$$

In these equations:

- BOA stands for “at the base of the atmosphere ”.
- TOA stands for “at the top of the atmosphere ”.
- A is the albedo of the shallow bottom , dimensionless.
- R is the reflectance of the shallow bottom measured at sea-surface , dimensionless.
- 2K is an operational two-ways attenuation term in units of m^{-1}, the sum of a down-welling term and an up-welling term.
- Z is the height of the water column, or depth of the shallow substrate, in units of m.

Preprints (www.preprints.org) | NOT PEER-REVIEWED | Posted: 6 June 2017 doi:10.20944/preprints201706.0030.v1

- 2K*Z is the optical depth, also called optical path length, dimensionless.
- LB is the spectral BOA radiance of the bottom substrate at null depth .
- LsB is the spectral TOA radiance of the bottom substrate at null depth; s stands for "at the sensor". The maximum TOA value for LsB, is noted LsM, for the maximum reflectance of a shallow bottom on site.
- Lw is the spectral BOA radiance of the sea where the bottom is optically deep, also called water volume reflectance, or backscatter.
- Lsw is the spectral TOA radiance of the sea where the bottom is optically deep; s stands for "at the sensor".
- L Is the spectral BOA radiance of the bottom substrate at depth Z.
- Ls is the spectral TOA radiance of the bottom substrate at depth Z; s stands for "at the sensor".
- La is the spectral radiance of the atmospheric path, measured from satellite altitude, also called path radiance.

Please note:

- Wavelength dependency subscripts of all L and K terms is omitted for brevity.
- 2K*Z : the two-ways optical path length, or optical depth, is dimensionless.
- Operational K: in the following, K and 2K are used interchangeably, for brevity. Replacing $K_{down} + K_{up}$ by 2K is a very practical simplification. This is discussed extensively by Maritorena et al. [17]; these authors conclude: "*The approximate formulae can be safely adopted in operation when interpreting or predicting the reflectance of shallow waters, in particular if Rw, and Kd have been estimated from remotely sensed data*".
- De-glinting: any contribution to the measured radiance by the haze, the atmospheric adjacency effect, or the sun/sky glint must first be removed.

It is very important to understand the inner workings of the simplified RTE. For that purpose, the following graphic illustrations of Figures 1a and 1b help to take control of how things work. This kind of graph is an exclusive and valuable bonus to the 4SM approach. They have been prepared using our 4SM code (see section 4.1), but may as well be prepared using a spreadsheet.

In the graphs of Figure 1, the Brightest Pixels Line (BPL) and the Soil Line are introduced: these terms shall be defined in sections 3.1 and 3.4. Values in Figure 1a are in relative radiances scaled to floating point the range 0-255; in Figure 1b, they are linearized by application of equation (7).

It should be noted that computing a multiple linear regression using existing depth data in empirical methods [1,2] amounts to placing a straight line at null depth in figure 1b, and use it as a radiometric reference model at null depth, somewhere over and in place of the curved Soil Line, with a slope and an intercept, and with all isobath lines being straight and parallel to that line. The consequences have been signaled in the introduction: depth under-estimation over bright and dark bottom substrates.

Preprints (www.preprints.org) | NOT PEER-REVIEWED | Posted: 6 June 2017 doi:10.20944/preprints201706.0030.v1

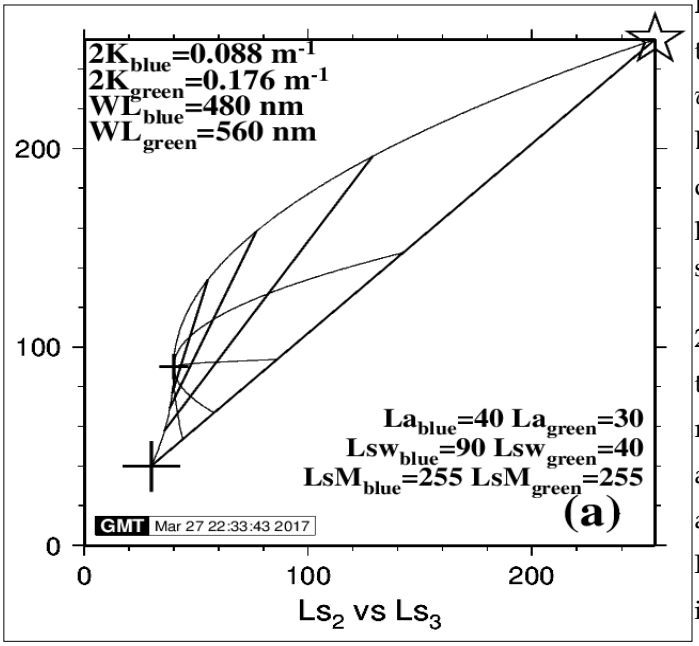

Figure 1 (a). Operating equation (5) at the top of the atmosphere: a plot of Ls_{blue} *versus* Ls_{green} in relative units. Star denotes LsM; small cross denotes Lsw; big cross denotes path radiance La. Six thin curved lines represent the exponential decay for six bottom types (LM_{blue}: 215, 107.5, 53.8, 26.9, 13.4, 0); the first is the BPL; two of them are darker than the deep water reflectance Lsw (small cross): they exhibit a negative bottom contrast where LB<Lw; and the last one represents a black body. Four thick straight lines represent four isobath lines: 0 (the Soil Line), 5, 10 and 15 meters.

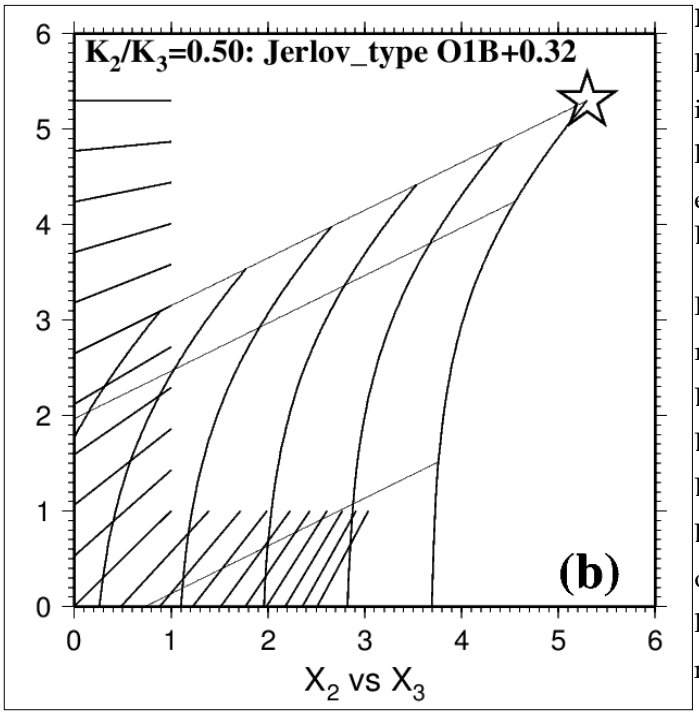

Figure 1 (b). Operating equation (8) for linearized data: a plot of X_{blue} *versus* X_{green} in logarithmic values. Three thin straight lines represent three bottom types: they exhibit a positive bottom contrast where Ls>Lsw; their slope is the ratio K_2/K_3, or K_{blue}/K_{green}. Six thick curved lines represent six isobath lines: 0 (the Soil Line), 5, 10, 15, 20 and 25 meters. The Soil Line is a curved line: this is because Lw_{blue} is distinctly stronger than Lw_{green}. But in the case of a Red *versus* NIR pair of bands, the Soil line would be a straight line, because Lw_{red} and Lw_{NIR} are both negligible.

Figure 1 (a,b). Plot of the simplified RTE. Band 2 is the blue band; band 3 is the green band. The values for La (big cross) and Lsw (small cross) have been set in order to convey a clear message in Figure 1a, rather than to be physically realistic.

Preprints (www.preprints.org) | NOT PEER-REVIEWED | Posted: 6 June 2017 doi:10.20944/preprints201706.0030.v1

All parameters of the simplified RTE are now written down and well understood, so that this model may now be inverted in order to retrieve the depth and spectral reflectance of the shallow bottom.

2.2. Inverting the model

Let LB_j denote the water column corrected radiance for the waveband j which suffered the strongest attenuation (like the red waveband). Let LB_i denote the average of all LB terms for wavebands i which suffered weaker attenuation (usually like all Blue-Green wavebands).

In the 4SM approach, inverting the model shall is done by increasing Z in (3), until the ratio LB_i/LB_j matches that of an operational radiometric model observed over land areas at sea level for the same band combination, namely the Soil Line which shall be introduced in section 3.1. As a practical measure, if all BOA radiance terms are normalized, then the slope of the Soil Line is conveniently scaled to 1; so that the inversion proceeds until the ratio LB_i/LB_j equals 1. Section 5.4 shall show that variants may be applied to this rule.

Several solutions may be operated to solve for spectral LB and depth Z, depending on the bottom contrast Ls-Lsw. In the case of a LANDSAT-8 image, and using only bands which exhibit significant bottom detection, a pixel may be modeled using

- either the NIR solution: $((LB_1+LB_2+LB_3+LB_4)/4)/LB_5$, (9)
- or the Red solution: $((LB_1+LB_2+LB_3)/3)/LB_4$, (10)
- or the Green solution : $((LB_1+LB_2)/2)/LB_3$, (11)
- or the Pan solution: $((LB_1+LB_2+LB_3)/3)/LB_{PAN}$. (12)

Please note that, if the Pan solution is used, it shall cover the whole depth range seamlessly: this all-important aspect shall be discussed at section 6.6.

3. Some new simplifying operational assumptions

Inverting the model requires the following four things, which can be estimated from the image itself:

- an operational spectral radiometric model of bare land areas at sea level, where depth Z is null;
- spectral Lsw ;
- spectral Lw ;
- spectral 2K .

Therefore, it shall be demonstrated that, apart from well accepted published information on the optical properties of marine waters [19] (table XVII), the 4SM approach does not require or use any reference to existing depth sounding data, or bottom substrate end member database for that matter.

Preprints (www.preprints.org) | NOT PEER-REVIEWED | Posted: 6 June 2017 doi:10.20944/preprints201706.0030.v1

3.1. The Soil Line

To estimate an operational BOA radiometric model of bare land from the image, let LBmax be the BOA reflectance of brightest bottom substrate at null depth, like over fine clean coral or quartz sand; and let LB=0 be the null BOA reflectance, like that of a black body at null depth.

The bare land pixels in the image at sea level, from brightest to darkest, are assumed to provide a suitable operational spectral model of bare shallow bottoms at null depth. This is intended to represent all shades of gray in the screen display of an enhanced color composite of the image, from black (LB=0) to white (LB=LBmax), and would plot as a straight line in a diagonal position in a bi-dimensional histogram of normalized BOA radiances.

In the case of a Blue *versus* Green bi-dimensional histogram, a greenish shallow bottom pixel at null depth, like a green vegetated pixel, would plot on the right hand side of the Soil Line in Figure 1a; see also the thick blue dot in Figures 5a, where the land pixels stand out on the right hand side of the Soil Line model. Of course, this shall be the cause of a possibly severe under-estimation of the retrieved depth unless something is attempted to alleviate this depth residual; and *vice-versa* for a blueish shallow bottom pixel. This aspect shall be discussed at sections 5.4 and 5.6.

3.2. Estimating Lsw

Estimating the TOA deep water radiance Lsw from the image requires that the area under investigation exhibits an area which is optically deep in all image bands. It also requires preliminary de-glinting, *i.e.* the removal of the contribution of the reflection of sky/sun light at sea-surface from the measured radiance of the marine pixels (see section 4.3).

3.3. Estimating spectral Lw and La

Equation (2) is for BOA radiances. It features Lw, the BOA spectral radiance of the sea where the bottom is optically deep. This term is assumed to be ~null over the Red-NIR range; but it is certainly not negligible over the Blue-Green range, as it determines the color of the sea.

An operational value of Lw is estimated through visual inspection of bi-dimensional histograms which exhibit the bare land pixels, and using some common sense. Then, remembering that Lsw is the TOA color of the optically deep sea after removal of any glint contribution, and that Lw cannot be negative, the atmospheric path radiance may be estimated as La=Lsw-Lw (6). This is discussed further at section 6.2.

3.4. The Brightest Pixels Line (BPL)

To estimate the ratio K_i/K_j of diffuse attenuation coefficients, the BPL is introduced as a radiometric model of the brightest bottom substrate LsM in the image over the full depth range.

The BPL represents the exponential decrease of the TOA radiance LsM as the bottom depth Z increases: this decrease is caused by the two-ways diffuse attenuation of the light flux through the water column.

Lyzenga observed in 1978 [1], that, in a bi-dimensional histogram of linearized data X=log(Ls-Lsw) for bands i and j, all pixels representing the same bottom substrate, *e.g.* homogeneous sandy bottoms at various depths, display along a straight line.

Preprints (www.preprints.org) | NOT PEER-REVIEWED | Posted: 6 June 2017 doi:10.20944/preprints201706.0030.v1

The slope of this straight line is the ratio K_i/K_j of the diffuse attenuation coefficients K_i and K_j. But Maritorena, 1996 [18], was not able to secure a faithful value of the ratio K_{green}/K_{gred} over coral reef sands from a SPOT image of the island of Moorea, French Polynesia, using a manual selection of homogeneous sandy bottom regions of interest at various depths as prescribed by Lyzenga: he then had to use a SPOT image of the island of Bora Bora, French Polynesia, where "*the lagoon is wide...supposed to have large homogeneous bottom zones*".

In contrast, it is observed that the brightest pixels in such a selection most often display as a straight line; this represents a significant variant of Lyzenga's method where the ratio K_i/K_j is established through linear regression of all selected pixels. Therefore the ratio K_i/K_j for all pairs of wavebands may be specified using an algorithm that selects the brightest pixel Ls_i for all pairs of pixels Ls_i and Ls_j in the shallow areas of the image. In other words, Lyzenga's observation applies to the brightest bottoms, which represent a physical limit of maximum brightness. As it turns out, this is mostly observed at isolated pixels rather than over extended supposedly homogeneous regions of interest, and may be verified by inspection of a screen display of the water column corrected reflectance. This allowed us in 1995 to process the SPOT 1 image of Moorea, as may be seen at http://www.watercolumncorrection.com/web-moorea.php.

It should be noted that all K_i/K_j ratios form a consistent suite, where $K_i/K_k=(K_i/K_j)/(K_k/K_j)$ for all pairs of K_i, K_j and K_k. Then, for the model to be inverted, a seed value is needed: this can be any of K_i or K_j, in units of m^{-1}.

3.5. Getting a seed value K_i in m^{-1}

Jerlov [19] (table XVII) proposed a classification of the diffuse attenuation properties for downwelling irradiance for marine waters worldwide under the following conditions: clear sky, sun high in the sky, very low content in suspended mineral particles. He points out that *"the spirit of this classification is that the irradiance attenuation coefficients Kd for any wavelength can be expressed as a linear function of a reference wavelength"*.

And Kirk [20] further commented: *"the reflectance spectra of oceanic waters vary in a roughly systematic way. A family of curves, of progressively changing shape, determined mainly by the phytoplancton concentration, is observed. Thus, for any given oceanic water, specification of the ratio of radiances or radiance reflectances at any two wavelengths, should in effect specify the whole radiance reflectance curve, and therefore the optical character of the water"*.

Over the years, using the ratio K_{blue}/K_{green} observed in the image, experience showed that spectral K for all visible bands (400 to 700 nm) may be interpolated from Jerlov's family of curves.

As it turns out,

- Blue-Green range: by application of spectral K, one obtains a tight fit of the slope K_i/K_j with the display of the brightest shallow pixels in a linearized bi-dimensional histogram for the pair of bands i and j in the Blue-Green range of the solar spectrum;

Preprints (www.preprints.org) | NOT PEER-REVIEWED | Posted: 6 June 2017 doi:10.20944/preprints201706.0030.v1

- UltraBlue range and Orange-Red range: spectral K must be distinctly reduced in these two ranges. This only became an evidence recently, by use of closely spaced quality hyperspectral bands of the HYPERION and then HICO sensors, and shall be presented at section 4.5;

- Self-calibration: in practice, all of many sea truth regressions allowed us to establish that depths retrieved in meters under such conditions only need tide correction.

In summary, the simplified RTE describes the exponential decay of the reflectance of a shallow bottom as its depth increases. In order to solve for both LB and Z in equation (3), the following new assumptions were introduced:

- In a bidimensional histogram of natural data, the Soil Line represents a spectral model of water column corrected reflectances LB.
- An optically deep area in the image is de-glinted and sampled in order to determine spectral deep water reflectance Lsw.
- Then an operational, and suitable, value of the spectral water volume reflectance Lw, and also of the spectral path radiance La, is derived by inspection of vegetated pixels in such bidimensional histogram for the pairs Blue *versus* Red and Green *versus* Red, and by using some common sense knowledge.
- In a linearized bidimensional histogram for the pair of bands i and j, with $K_i<K_j$, the ratio K_i/K_j is measured as the slope of the display of the brightest linearized pixels in band i for the whole range of linearized values in band j.
- Then this ratio for the Blue versus Green pair of bands is used to interpolate K_{blue} and K_{green} using Jerlov's data. It follows that, in the end, K is specified for all other visible bands.

Now that all aspects of the 4SM approach have been presented (its equations, and the new assumptions), we proceed to explain how to work out all parameters that are needed to specify the simplified RTE (optical calibration) for the specific image to be processed.

4. Materials and Methods

For this presentation, the following material used (see Figure 2a-c):

- (a) a LANDSAT-8 multispectral 180 km wide image over Oceanic waters at Lee Stocking Island, Bahamas: scene LC80120442014029LGN00 dated january 29th 2014, downloaded from USGS Earth Explorer (https://earthexplorer.usgs.gov/). It is used for details of the calibration process in Figure 4.
- (b) a HYPERION hyperspectral 15 km wide image subset over Oceanic waters in the Tuamotu archipelago: accross the atoll of Fakarava, French Polynesia, scene EO1H0510712011264110TX_SGS_01 dated september 21rst 2011, downloaded from USGS. It is used in sections 4.5 and 4.6, Figures 5, 6 and 7.
- (c) a sea truth digital terrain model (DTM, 120 km wide) at 30 m ground sampling distance (GSD) of Caicos Bank, Bahamas, was purchased over the Internet from Harris-Ellis_Knowledge_Transfer project [23]; it may be inspected at http://www.watercolumncorrection.com/images/c/cai/caicos_DTM_harris-ellis.png. It shall be used in Figure 8 at section 5.5, to evaluate the sea truth on depths retrieved

Preprints (www.preprints.org) | NOT PEER-REVIEWED | Posted: 6 June 2017 doi:10.20944/preprints201706.0030.v1

using LANDSAT-8 scene LC80090452014312LGN00 dated November 8th 2014, downloaded from USGS.

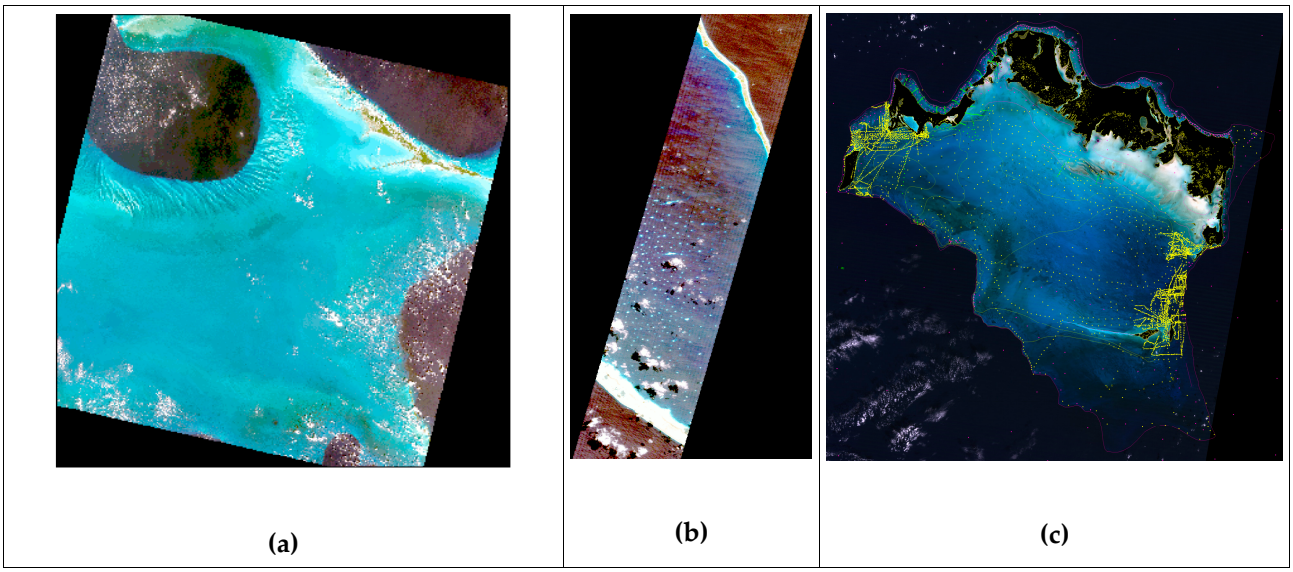

(a) **(b)** **(c)**

Figure 2. Three images used to prepare the illustrations. **(a)** LANDSAT-8 over Lee Stocking island, Bahamas; **(b)** HYPERION over Fakarava atoll, French Polynesia; **(c)** LANDSAT-8 over Caicos Bank, Bahamas: yellow points show the scatter of depth sounding points used by Morgan and Harris [23] to prepare their DTM.

4.1. The 4SM code, and its performance

We use the following open source resources:

- OpenEV (http://openev.sourceforge.net/), as a lightweight image viewer, to export the raw data (usually a TIF file) into a PCIDSK formated file, and to create shapefiles;
- system calls by 4SM code to GMT, the Generic mapping Tool (https://www.soest.hawaii.edu/gmt University of Hawaii) to prepare PostScript files, and to Ghostview to display PostScript files on screen.

Apart from the above open source resources, we only use our own 4SM code written in C on a x86_64 full HD notebook under Linux. This code was developed over the last twenty years as an ergonomic one-stop "do it all" proprietary code, under the control of one single command line bash script and a close supervision by the practitioner, with the following work flow which covers all aspects of our work, as presented at http://www.watercolumncorrection.com/4sm-flowchart.php:

- import (and re-sample as appropriate) raw data into a working File interleaving PCIDSK formated database;
- run through a series of preparations which include UTM georeferencing of that database, reading and using shapefiles, recoding of rasters and production of masks, optical calibration of the RTE, *etc*;
- then, once satisfied with these image preparations, read up to in excess of twenty six spectral bands, line after line,

Preprints (www.preprints.org) | NOT PEER-REVIEWED | Posted: 6 June 2017 doi:10.20944/preprints201706.0030.v1

- and proceed "on the fly", for each line, to de-glinting, pan-sharpening if required, smart-smoothing if required, and then inverting the simplified RTE,
- to produce a raster of SDB, several rasters of de-glinted bands, and several rasters of water column corrected bottom reflectance ready for bottom typing.

The code also includes bottom typing, profiling, and sea truth services, and other minor utilities.

As regards performances on a 64 bits 2.4 GHz Intel I7 Core laptop, this code processes the 16.7 millions pixels of the Caicos Bank LANDSAT-8 seven bands study case of Figure 8 in 3.1 minutes (that is 89,600 pixels per second), or a 17 bands 36 millions pixels 1 m GSD CASI image of Heron Island, Great Barrier Reef, in 54 minutes.

Processing of two full LANDSAT-8 scenes at a 15 m pan-sharpened GSD is customarily done in just one one day. This allows to undertake time series study cases, in comfortable conditions, to produce a final clean combined depth SDB, free of transient adverse local conditions or areas of no data, which does not need any smoothing, at a 15 m GSD. This is presented in another paper [14].

4.2. Image preparation

All that follows is done using the 4SM code. First the raw data is imported as raw DNs into a working image database. If a panchromatic band is available, either it is oversampled and added to the multispectral bandset (*e.g.* for a 30 m GSD LANDSAT-8 7seven bands study), or the multispectral bands are undersampled and the panchromatic band is added to the multispectral bandset (*e.g.* for a 15 m GSD LANDSAT-8 seven pan-sharpened bands study); pan-sharpening results in some beneficial smoothing. In the case of a hyperspectral image, a synthetic panchromatic band is prepared as the convolution of radiance signal in each multispectral band i with the panchromatic response at wavelength WL_i . Then, it is scaled as appropriate and added to the set of multispectral bandset (*e.g.* for a 30 m GSD Hyperion study).

Once the raw data is imported in a working database, and for each processing run, the raw 16 bits data is accessed, scaled as floating points, de-glinted as required (some images do not require de-glinting, or cannot be de-glinted), smoothed if required, pan-sharpened if required, and finally processed as required on the fly , line by line, under control of the command line script.

Optical calibration requires the interactive preparation of a mask to delineate land from water. Shapefiles are prepared to mark out unwanted areas, alien floating objects, and regions of interest (ROI) where to sample the glint, the deep water reflectance, some brightest bare land, and some healthy vegetation.

4.3. De-glinting

De-glinting uses the process described by Hedley et al. [21], which assumes a null penetration in water of the NIR-SWIR bands of the spectral images. A sample of marine pixels over optically deep water areas affected by a variable amount of sun or sky glint (or by lumps of haze, or even by atmospheric adjacency effect) is collected in order to perform the linear regression of all visible bands against the NIR or SWIR band. Then the amount of "glint" in visible bands is evaluated and subtracted using these regressions. The result is illustrated in Figure 3, which presents a WORLDVIEW-2 image in the Red band over the Gulf of Laganas, Zakynthos island, Greece,

Preprints (www.preprints.org) | NOT PEER-REVIEWED | Posted: 6 June 2017 doi:10.20944/preprints201706.0030.v1

acquired August 22nd 2014. There appears to be no wind, as the sea surface is not affected by any wave modulated glint, or wind generated clutter. But the image exhibits a very strong atmospheric adjacency effect, which is efficiently removed through the de-glinting process: for a comparison, the central stripe has been left un-corrected.

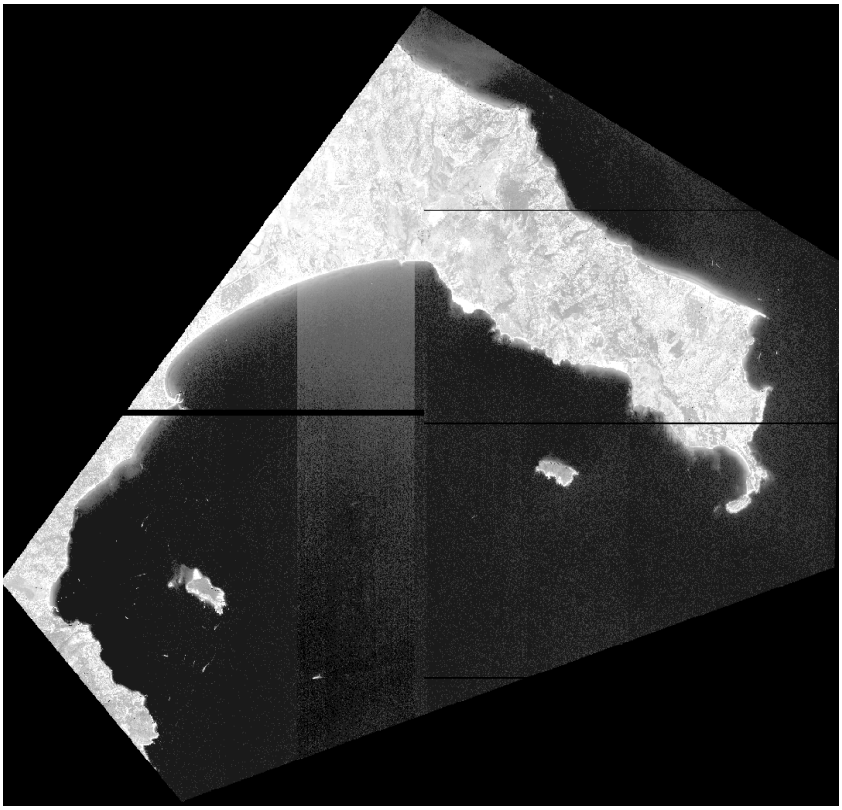

Figure 3. It shows the removal of the atmospheric adjacency effect by the de-glinting process. This scene exhibits some lines of missing data. This image is 16 km across. See text for explanation.

4.4. Extraction of the calibration data

The mask and various shapefiles are used to ensure that only the desired areas or ROIs are sampled for calibration data: "clean" marine pixels are wanted. This extraction is done for whole image, or through a mask, or limited to a sub-window. To extract the BPL pixels for the pair of bands i and j with $K_i<K_j$, , for each Ls_j the pixel with the highest Ls_i is selected along with its position in the image. This forms the BPL pixels for that pair of bands. It is at times useful to enable smoothing. Bi-dimensional histograms (BDH) are extracted for all pairs of bands i and j with $K_i<K_j$. Marine pixels can be raw or de-glinted. The BDH can be complete or marine areas only, or even land only. In the end two calibration data text files are written, one for the BPL data, and one for the BDH data.

Upon the first operation, a provisional "auto-calibration" command line script is formatted: it offers default or rough estimate values for the desired parameters; the auto-calibration graph is displayed automatically on screen.

The calibration data for the specific image to be processed are now available as text files: sections 4.5 and 4.6 detail of how they are used to work out the complete set of spectral parameters

 doi:10.20944/preprints201706.0030.v1

that are necessary to specify the simplified RTE for visible bands. This usually takes less than one hour for a LANDSAT-8 image.

4.5. Optical calibration for the multispectral bands

Then these preliminary command line script values must be edited and modified in that script by the practitioner as appropriate, and a new calibration run is launched automatically upon closing the screen display of the previous calibration run, until satisfied. These parameters form the backbone of the command line script. This step requires all the attention of the practitioner.

- Ratio K_{blue}/K_{green} : must be adjusted manually.
- LsM: must be adjusted manually together with the K_{blue}/K_{green} value, so as to ensure a nice fit of the BPL model with the scatter of BPL pixels.
- As for visible bands other than Blue and Green, their K and LsM values must be adjusted manually.
- Lsw: choosing the location where to estimate the deep wter reflectance is of the utmost importance. De-glinting is essential; spectral profiling across the image may help refine this choice.
- Lw: because La=Lsw-Lw, the choice of Lw, along with that for LsM, completes the specification of the Soil Line. For this, one conveniently remembers that Lw may be considered negligible over the red range, as it is for a NIR or SWIR band; and that dense healthy vegetation pixels should plot (i) on the Soil Line for a Blue/Red pair of bands because both Blue and Red are darker than Green, and (ii) on the green side of the Soil Line for a Green/Red pair of bands.

The optical calibration for multispectral bands is illustrated in Figures 4-6.

Preprints (www.preprints.org) | NOT PEER-REVIEWED | Posted: 6 June 2017 doi:10.20944/preprints201706.0030.v1

Figure 4 presents the calibration diagrams for the pair Blue/Green for the LANDSAT-8 scene LC80120442014029LGN00, Jan 29th 2014, over Lee Stocking Island, Bahamas: the bi-dimensional diagram represents all image pixels; all marine pixels are de-glinted. It is observed that the scatter of BPL pixels in the plot of linearized data of Figure 4b forms a fairly straight line with a slope K_{blue}/K_{green}~=0.52 over the whole 0-30 m depth range for bright bottom substrates: waters appear to be homogeneous. This value of K_{blue}/K_{green}~=0.52 forms the basis of the so-called "self-calibration" : using this value, spectral K for all visible bands are then estimated in units of m^{-1}: K_1=0.099; K_2=0.093; K_3=0.179 and K_4=0.675. Please note that K_4 for the red band had to be forcibly reduced from 0.795 to 0.675 m^{-1} in order to secure a good fit of the BPL line (this shall be discussed later in this section). Still, the plot of natural data exhibits distinct bumps: these indicate that things might actually be not so simple after all; and it must be noted that this process may hide areas of less clear waters for which the ratio K_{blue}/K_{green}>>0.52. It is also clear in Figure 4b that the maximum optical path 2K*Z (in other words the maximum depth of bottom detection) decreases drastically as the bottom brightness decreases.

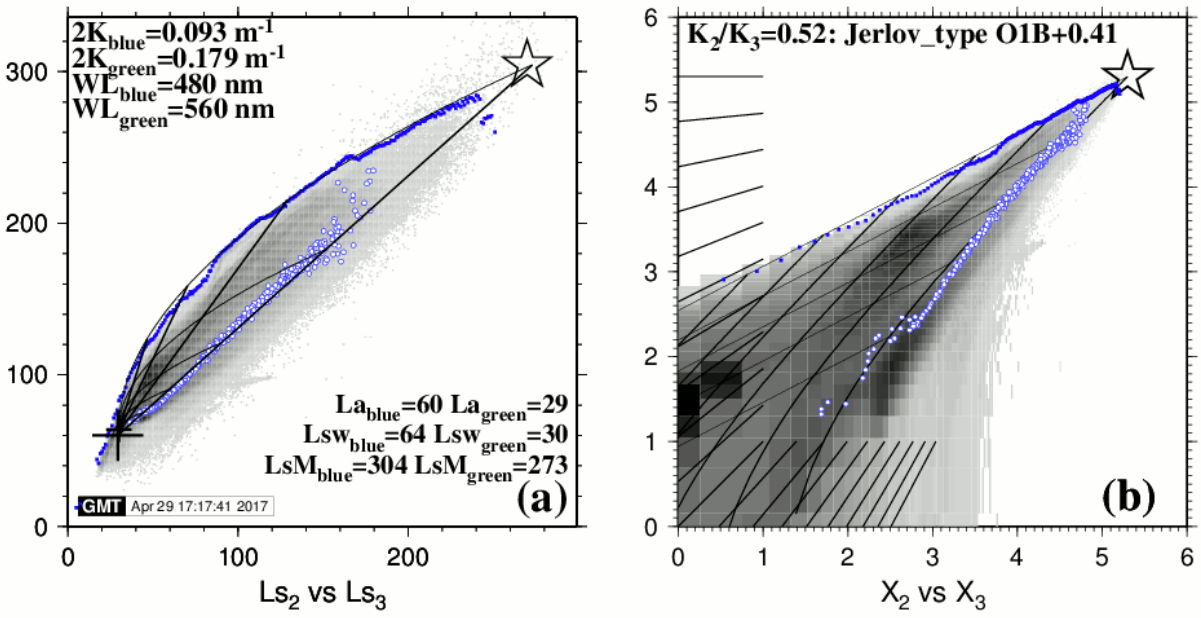

Figure 4. Calibration diagrams for the pair Blue/Green for the LANDSAT-8 image: Blue *versus* Green. Band 2 is Blue; band 3 is Green. The ratio K_{blue}/K_{green}=0.52. The backdrop in shades of gray represents the bi-dimensional histogram for all image pixels. Blue dots: the BPL pixels are real pixels, each referenced to its row/line position in the image. Small white circles represent the scatter of averaged bare land pixels, as a proxy for the Soil Line. The value of select parameters are provided; **(a)** shows the natural calibration data; **(b)** shows the linearized calibration data. Thick lines: six isobath lines are drawn: 0, 5, 10, 15, 20 and 25 m. Thin lines: five isobottom lines are drawn.

Preprints (www.preprints.org) | NOT PEER-REVIEWED | Posted: 6 June 2017 doi:10.20944/preprints201706.0030.v1

At this stage, all K values have been estimated for visible bands, but close inspection of the calibration graph leads us to question the value for $K_{red.}$, which had to be reduced forcibly from 0.795 to 0.675 m^{-1} . This specific matter raises serious questions, and is now investigated in Figure 5. Figure 5 presents the calibration diagrams for various pairs of bands for the HYPERION hyperspectral image. 25 bands in the visible range were used. Band 4 is blue; band 11 is green; band 21 is red, and band 24 is far red. This figure illustrates the need for decreasing the operational 2K over the orange-red region of the solar spectrum, which was signaled earlier. This is now an established fact which was observed using spaceborne hyperspectral images, first using HYPERION data at the atoll of Fakarava, then later confirmed using HICO data at Lee Stocking Island, Bahamas. This, after years of searching for an explanation, provided overwhelming evidence as to how to interpret the lousy fit customarily observed for the red band when using multispectral data.

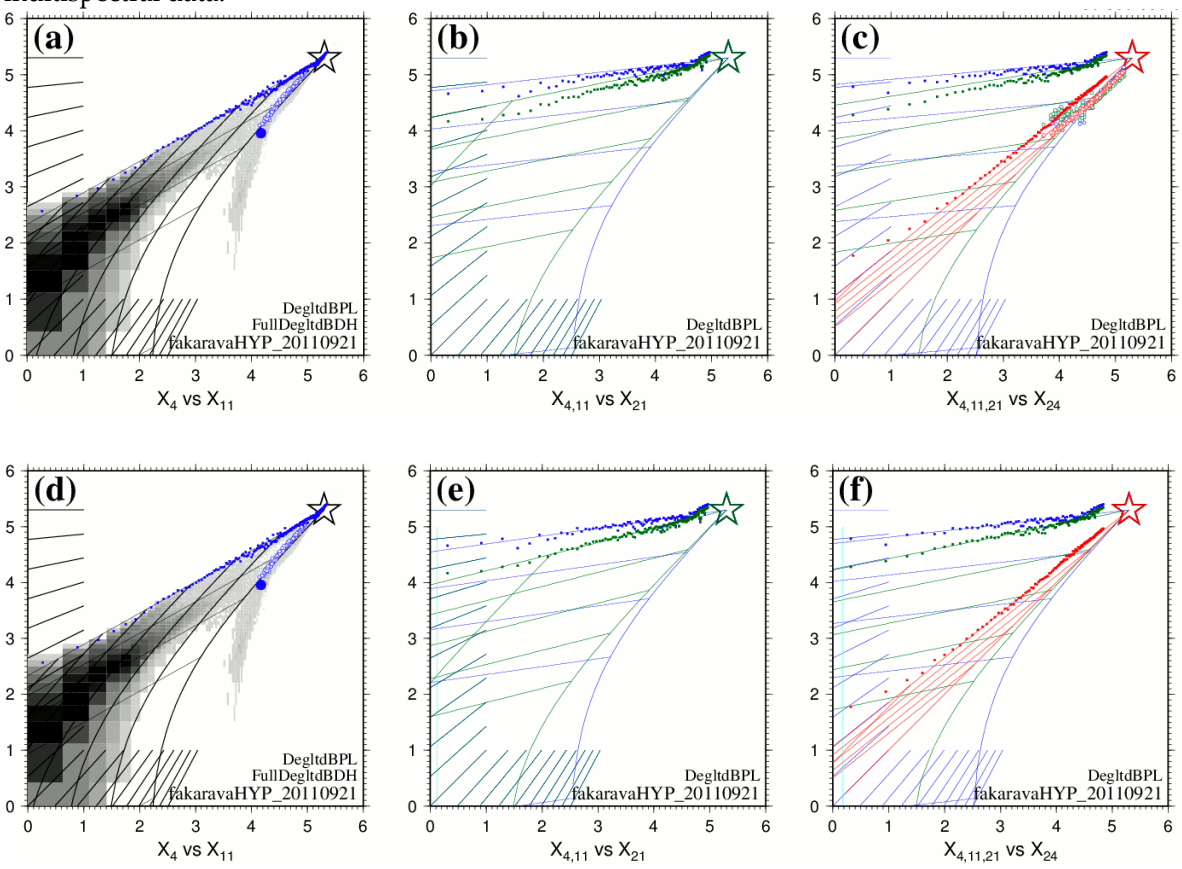

Figure 5. Calibration diagrams for various pairs of bands for the HYPERION image. The ratio K_{blue}/K_{green}=0.56; **(a-c)** illustrate a bad fit: K_4=0.089, K_{11}=0.159; K_{21}=0.769; K24=0.960; **(d-f)** illustrate a good fit: K_4=0.089, K_{11}=0.159; K_{21}=0.626; K_{24}=0.781. Plots (a,d) show that the BPL displays as a straight line for the Blue/Green pair. Plots (b,c) exhibit a bad fit of the BPL model with the scatter of BPL pixels: both K_{21} and K_{24} must be reduced forcibly in order to achieve a satisfactory fit: this is achieved in plot (e) for band 21 and in plot (f) for band 24.

Because the calibration data extraction process picks the brightest pixels in band i, it tends to pick up noisy pixels which plot distinctly above the BPL model at great optical path 2K*Z, *i.e.* near

Preprints (www.preprints.org) | NOT PEER-REVIEWED | Posted: 6 June 2017 doi:10.20944/preprints201706.0030.v1

extinction of the bottom contrast Ls_j-Lsw_j: this may be observed in Figure 5e, and is just an expression of the S/N properties of the image and of the de-glinting process.

Figure 6 presents 2K curves in m^{-1} for all water types of Jerlov's classification, from Oceanic I to Oceanic III (violet to green curves), then from Coastal 1 to Coastal 9 (green to yellow curves). The black curve represents the observed operational spectral 2K for the HYPERION image of the atoll of Fakarava: water type OIB+0.49 for ratio K_{blue}/K_{green}=0.56; white circles along the black line present the scatter of 25 values for observed operational 2K: these values have been decreased manually over the orange-red range of the solar spectrum, in order to achieve a good fit of the optical model with the BPL pixels. Note that the need for such manipulation increases regularly from orange bands to far red bands, thus indicating a possible link with diffuse properties of the radiance field measured by the sensor's telescope. This of course raises interesting questions which shall be formulated in section 6.3.

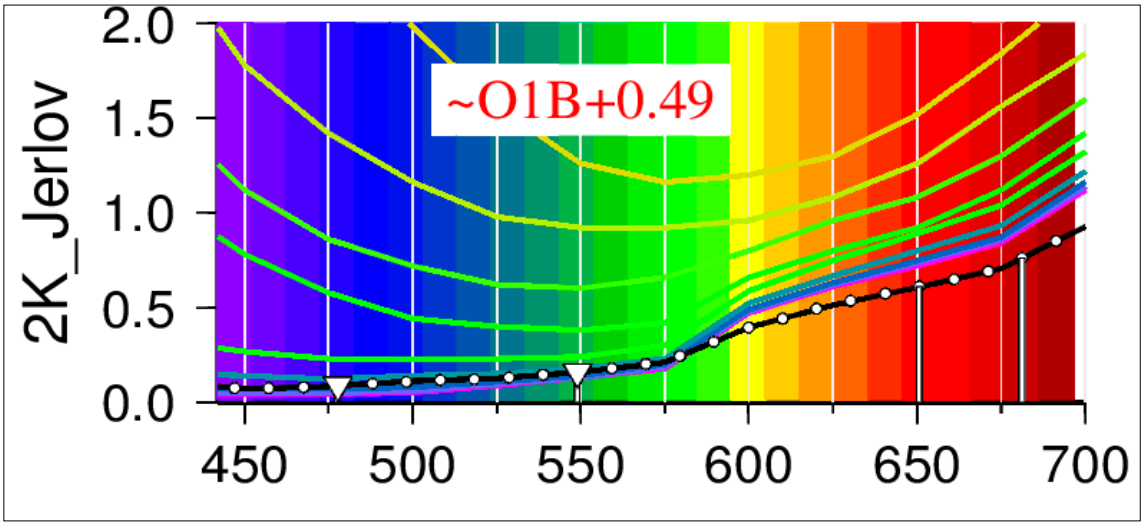

Figure 6. This graph presents 2K curves in m^{-1} , for all water types of Jerlov's classification, along with the observed curve for the HYPERION image (black with white dots), versus wavelengths in nanometers. Please note the sharp increase between 575 and 600 nanometers for Oceanic waters.

4.6. Optical calibration for the panchromatic band

A panchromatic band is specified by its response curve, which covers a specific portion of the visible-NIR range. Therefore, its diffuse attenuation coefficient K_{PAN} may be expected to decrease more or less regularly as the water depth Z increases. This translates graphically into a curved linearized BPL model. This curve is specified as a function

- of the panchromatic response curve,
- and of K_{blue} over the whole depth range.

Preprints (www.preprints.org) | NOT PEER-REVIEWED | Posted: 6 June 2017 doi:10.20944/preprints201706.0030.v1

This is illustrated in Figures 7a,b. Band 4 is blue; band 11 is green; band 21 is red, and band 25 is PAN. Thick lines: isobath lines are shown for both plots: 0, 5, 10, 15, 20, 25 (and 30 m in Figure 6a); isobath lines are regularly spaced in (a), but not so in (b): the panchromatic solution should therefore yield more detailed results at shallow depth than the Green solution.

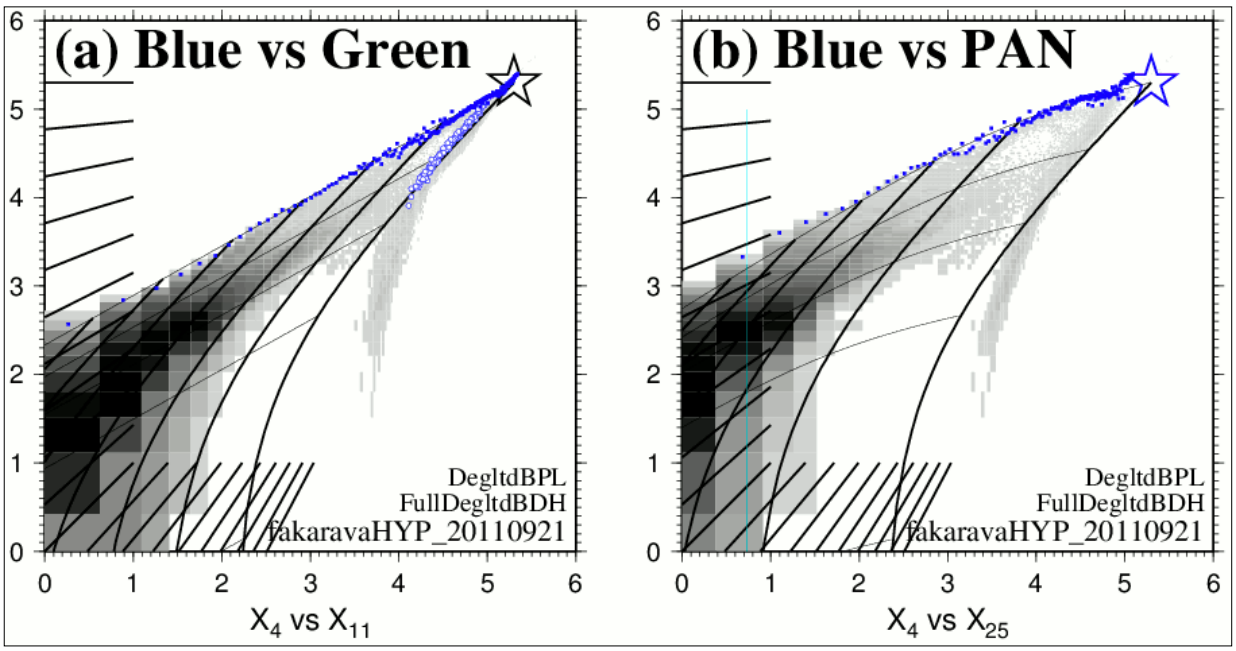

Figure 7. Calibration of the synthetic panchromatic band for the HYPERION image. The ratio K_{blue}/K_{green}=0.56. Thick lines: six isobath lines are drawn: 0, 5, 10, 15, 20 and 25 m. Thin lines: five isobottom lines are drawn. **(a)** the plot of X_4 *versus* X_{11} is for Blue *versus* Green, same as above in Figure 5, for a visual comparison: both the BPL pixels and the BPL model display as a straight line; **(b)** the plot of X_4 *versus* X_{25} , or Blue *versus* PAN, shows the calibration of the panchromatic band which is placed in channel 25: both the BPL pixels and the BPL model display as a curved line, with a very nice fit.

4.7. Iterations and fine tuning

The optical calibration of the simplified RTE is now secured. But it is often the case that some local conditions depart notably from the overall picture. It is important that the practitioner investigates such odd situations in order to refine the choice of spectral deep water radiance, or the spectral threshold to be applied to radiances. This may be done by displaying the spatial variations of spectral raw and/or de-glinted radiance using a profiling routine available in the 4SM code. This is very much part of the calibration process and should not be overlooked for sake of expediency.

5. Results: sea truth on retrieved depths

In the end, all parameters that are necessary to specify the simplified RTE for visible bands are available, and the image may be processed. The RTE is inverted using equation (3) and the PAN solution (see section 2.2), without any smoothing. We shall now elaborate on the sea truth

Preprints (www.preprints.org) | NOT PEER-REVIEWED | Posted: 6 June 2017 doi:10.20944/preprints201706.0030.v1

evaluation of the depths retrieved by the 4SM approach (SDB). The main purpose of this evaluation is to test the assertion that there is no need for field data to calibrate the simplified RTE.

The existing sea truth DTM raster of Caicos Bank, Bahamas (that was purchased over the internet, see Figure 2c), is used to evaluate the SDB obtained using LANDSAT-8 scene LC80090452014312LGN00 dated Nov 8th 2014 at 30 m GSD, over the 0-30 m depth range. This image subset is ~120 km wide, 4018 rows and 4149 lines: that is 16.7 millions pixels. Shallow bottoms at Caicos Bank are commonly covered in turtle grass; they also exhibit areas of very bright oolith sands.

5.1. Sub-sampling and masking

In respect of this study, this coarse DTM is found wanting :

- depths appear to be over-estimated in the 1-2.5 m depth range, as can be seen in the sea truth histogram of Figure 8b;
- the 3-6 m range is prominent;
- the 15-30 m depth range is poorly represented as the bottom drops suddenly to the deep;
- several areas lack depth points in sensitive surroundings such as clusters of isolated shoals, and in the 15-30 m range;
- no water depth datum is available for this DTM, and tide height is unknown, although it should not exceed 0.8 m. As it turns out, a tide height of 0.5 m appears to suit the situation.

Nevertheless, it shall be very useful, subject to the following manipulations which are necessary for the Root-Mean-Square Error (RMSE) on SDB depths to mean anything.

In practice, first, a mask is used to exclude areas where (i) the sea truth DTM raster exhibits coarse triangular interpolation patterns in the raster, (ii) the LANDSAT-8 image exhibits scatters of very small clouds/shadows.

For this exercise, and because the project area is so vast at 15 m GSD, one in three lines and one in three columns are read; that is one in nine pixels. Pixels which do not exhibit both DTM depth and SDB depth are also excluded: this results in a total of 581,982 pixels (or depth pairs) to be evaluated, which therefore represent 5,237,838 raster nodes (or depth pairs).

5.2. Thresholding the outliers

Then the 5,237,838 accepted depth pairs (in units of centimeters) are assigned to decimeter bins. Some bins count many pairs (like in the 30 to 60 decimeter depth range); they form the main body of data to be regressed and shall be plotted from black to white as thick points in the bi-dimensional regression of Figure 8a. But other bins count very few pairs: these are outliers and shall be plotted as thin gray points. Outliers occur for many different reasons and must be excluded from the regression. For example, bad areas in the DTM (coarse spacing of depth sounding) , or in the image (clouds and their shadows), are flagged using a mask and excluded from the regression. Moreover, depth bins which count too few pixels are also flagged using a threshold and excluded: in practice, a threshold of 2 pixels is enforced, *i.e.* pairs with less than 3 occurrences are flagged and excluded.

Preprints (www.preprints.org) | NOT PEER-REVIEWED | Posted: 6 June 2017 doi:10.20944/preprints201706.0030.v1

5.3. Sea truth regression

Finally, all accepted pairs are binned into meters and averaged: they are represented by stars and circles in Figure 8a: from 0 to 12 m, these averages display well along the diagonal (stars). In contrast, deeper than 12 m, other averages are mostly outliers which must be discarded (circles). This 12 m threshold depth is determined as follows: starting from 0 m, all accepted pairs are counted by order of increasing DTM depth until a total of 99% of all accepted pairs is reached. This yielded 12 m. In other words, DTM depths in excess of 12 m only account for 1 % of all accepted pairs for this scene (circles). By application of this threshold, the regression now is faithfully representative of the 4SM approach over the 0-12 m depth range for one single LANDSAT-8 image in the Bahamas: allowing for a tide correction of 0.5 m on DTM_depths, the following regression is obtained

$$SDBdepth = 0.35 + 0.96 \square DTMdepth,\ N = 4.6\,million,\ R2 = 0.89,\ RMSE = 0.81\,m \quad . \qquad (13)$$

Inside the gray polygon of Figure 8a, retrieved depths which are within +/-1 m of DTM depth amount to 89.6% of all black to white points.

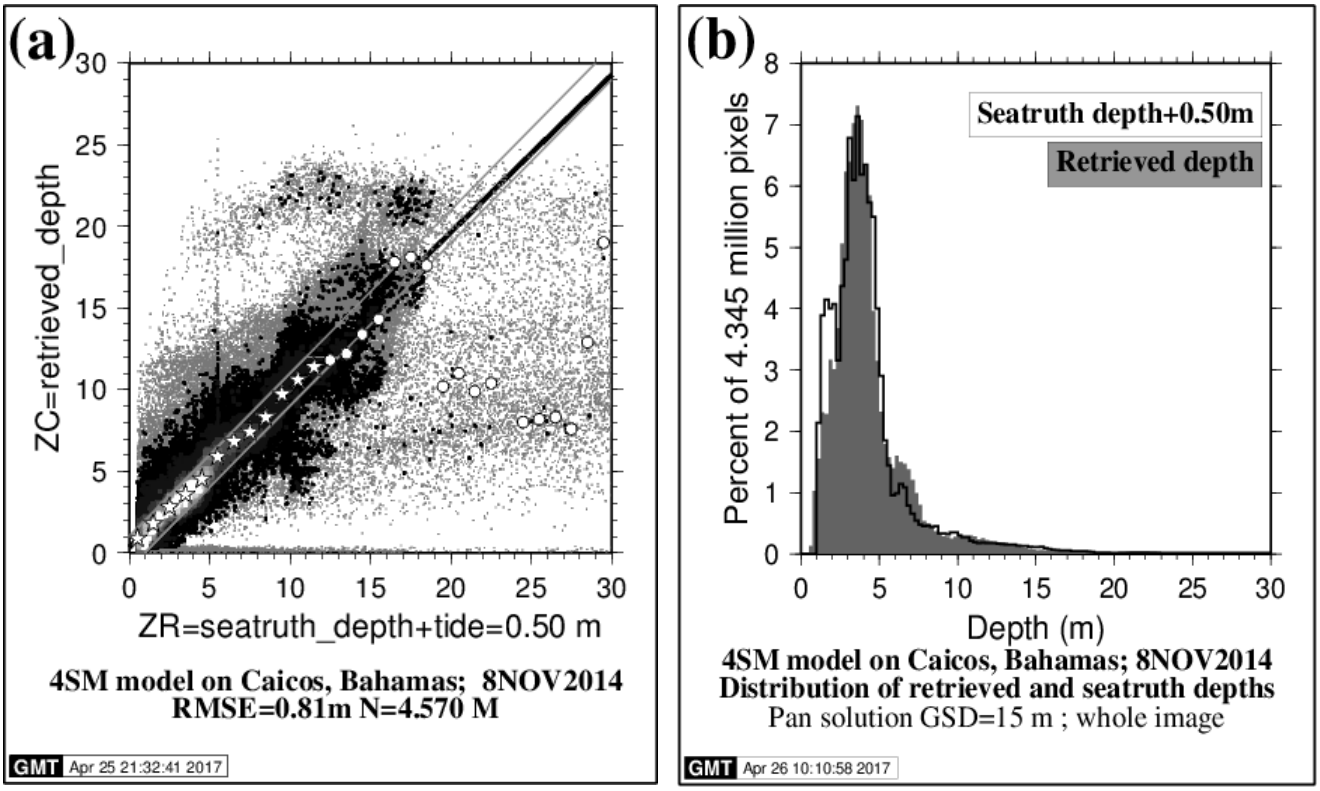

Figure 8. Sea truth regression of SDB versus DTM depths for the Caicos Bank study case: **(a)** Plot of retrieved depth versus sea truth depth, allowing for a 0.5 m tide height; thin gray points are excluded from the second regression; **(b)** Overlay of histograms of retrieved depths and sea truth depths; both histograms account for all depth points used in first regression.

 doi:10.20944/preprints201706.0030.v1

5.4. Learning from the RED solution: using a LUT

One must question the cause of the wide scatter of points off the diagonal in Figure 8a. In the 4SM approach, inverting the RTE relies on the Soil Line assumption, which can only yield under-estimated retrieved depths over green shallow substrates (which cover most shallow bottoms at Caicos Bank) when using either the Green solution or, to a lesser extent, the Pan solution. In order to alleviate this problem, one may first learn from the results obtained by using RED solution a way to adjust the Green and the Pan solutions in order to improve the results for a majority of pixels, and write this knowledge into a look-up table which is hard-coded in the 4SM code, then use this LUT in place of the original Soil Line. This device turns out to be quite beneficial in producing a less biased scatter of points in the bi-dimensional regression histogram. These depth residuals affect areas in the image rather than pixels at random (see an illustration in section 5.6). Therefore, they are not noise-related, but rather represent spatial variations in the spectral properties of the bottom substrate or of the optical properties of the water, which are not accounted for by the inversion scheme. This is inevitable, and should reveal to be linked to variations of the local conditions of the bottom substrate through space and/or time, such as life and death of biofilms, seasonal vegetation cycle, *etc*, and, in the case of the Bahaman karstic shelf, bursts of black ground water seeping up from the shallow brackish water table.

5.5. No need for field data

Applying a smart smoothing scheme upon running the inversion of the RTE does result in lesser scatter of points in the bi-dimensional regression histogram. Restricting the depth range to 3-17 m should also reduce the root mean square error (RMSE) on retrieved depths, because the 0-3 m depth range is over-represented in the DTM, as shown by the sea truth depth histogram of Figure 8b.

In the end, Figure 8a shows that, allowing for a 0.5 m tide height, depths retrieved in the 1-18 m depth range by use of the spectral 2K derived from the image itself are very close to the sea truth data. This is demonstrated by the quasi-diagonal scatter of 89.6% of all depth pairs, where retrieved depths are within +-1 m of sea truth depth. So far, this proved to apply to clear waters for all airborne/spaceborne hyper/multi-spectral imageries.

As for Figure 8b, it shows that the DTM exhibits an excess of depth points in the 1-2.5 m depth range.

Therefore, in a large majority of study cases, it is demonstrated that, using the 4SM approach, there is no need for field data, nor for formal atmospheric correction, to calibrate the RTE and compute depths in meters: these depths then only need a tide correction.

5.6. Depth residuals

Retrieved depths are computed in centimeters. By subtracting the SDB depths from the tide-corrected DTM depths, one obtains a raster of the depth residuals. This is presented in figure 9. It can be seen that over- or under-estimation of depth affects areas, rather than individual pixel. Some areas are badly affected by clutters of small clouds and their shadows, and some odd dark blue areas are affected by erratic interpolation in the DTM.

Preprints (www.preprints.org) | NOT PEER-REVIEWED | Posted: 6 June 2017 doi:10.20944/preprints201706.0030.v1

But it may be seen all along the reef rim all along the northern edge of Caicos Bank, that many dark blue areas exhibit badly over-estimated depths while some dark red areas exhibit badly under-estimated depths: these reef rim areas depart from the vast bank which is covered in turtle grass (see section 5.4). Much more need to be investigated in order to try and alleviate these discrepancies, as the Soil Line assumption is certainly not a match to a spectral library of bottom substrate spectral reflectance signatures representative of the site.

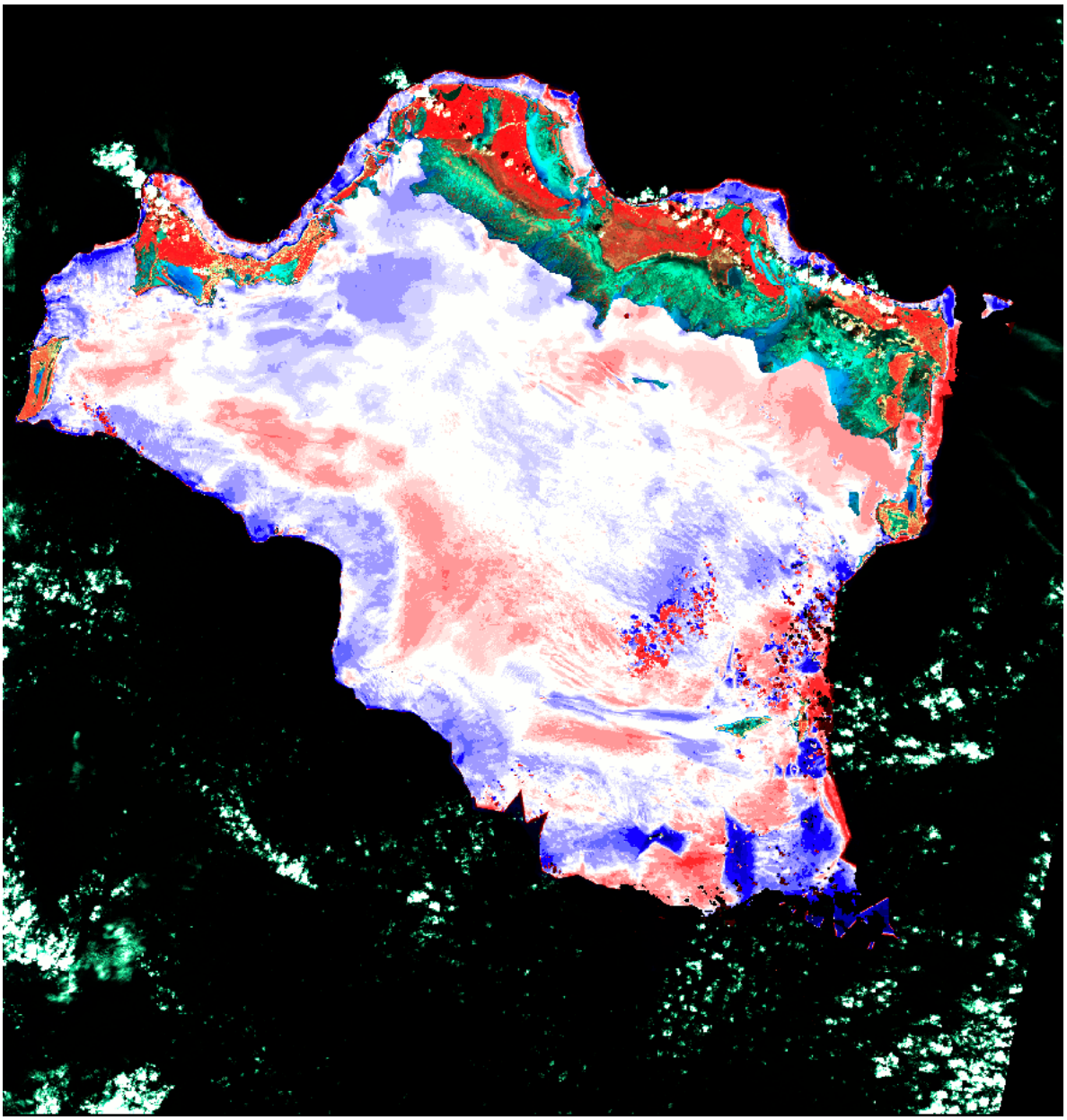

Figure 9. It presents the overlay of the depth residuals ZDTM-ZSDB over a false color composite. Changes in color are by steps of 0.25 m (0-1 m, light hues), then by steps of 1.0 m (darker hues). Residuals less than +/- 0.25 meters are mapped in white. Blue hues represent areas of over-estimated depths. Red hues represent areas of under-estimated depths.

Preprints (www.preprints.org) | NOT PEER-REVIEWED | Posted: 6 June 2017 doi:10.20944/preprints201706.0030.v1

6. Discussion

Remote sensing of the ocean color over an optically shallow bottom involves the equations which describe the fate of a photon from the sun to the water surface, then down through the water column to the shallow bottom, then up through the water column, then up to the remote sensor's very narrow field of view: this is the domain of analytical methods and very advanced sensors. Analytical methods rely on a database of spectral bottom substrate reflectance, possibly obtained *in situ*, and aim at producing an exact solution for depth, spectral K, and water column corrected spectral bottom reflectance[15].

For sake of operationality, empirical methods have been devised in order to make use of available and affordable imagery, which have all been specified for land areas, like LANDSAT. Therefore, empirical methods overlook much of the analytical complexities. To this date, they all rely on existing *in situ* depth soundings to retrieve the shallow bottom depth, and do not produce the most desired water column corrected spectral reflectance of the bottom substrates which would allow for bottom typing.

After all, one must to keep in mind that SDB can be useful even though the retrieved depths are biased to some extent, and that bottom typing depends on the separability of water column corrected bottom spectral signatures much more than on exact signatures.

Therefore, the relevant question here is: what are the shortcomings of a simplified RTE approach, and do they impair the results to the point that SDB becomes useless and bottom typing a vain quest?

It must be stressed that this discussion assumes clear waters, with a negligible water leaving reflectance over optically deep waters in the NIR-SWIR range of the solar spectrum. Significant progress in underway to accommodate less favorable water quality conditions [24], where an atmospheric correction model is used to derive the glint correction algorithm.

6.1. De-glinting, deep water reflectance Lsw, and the bottom contrast

First, it must be acknowledged that some images exhibit such atmospheric or sea-surface complexities that they must be discarded altogether. Otherwise, in the absence of distinct wind-generated glint clutter at the water surface, glint regressions are prepared using lumps of haze or even atmospheric adjacency effect over deep water. A good de-glinting using the Hedley et al. protocol [21], which is based on the dark pixel assumption in the NIR band, produces an even radiometric spectrum over deep water areas: this is the condition for estimating the all-important deep water radiance terms Lsw and Ls in the RTE (4).

This de-glinting protocol proved to efficiently remove the swell modulated and adjacency effect components of the marine signal, but not the sky dome component which is constant, *i.e.* not modulated by the swell or water surface glitter. This is not a problem, though, as the sky dome component affects both Ls and Lsw terms. Therefore the bottom contrast Ls-Lsw is not affected. As a result, and in most cases, the simplified RTE approach does not require a formal atmospheric correction.

The optical depth limit for inferring bathymetry, also known as the extinction depth, is ~30 m in the sea truth case at Caicos Bank (section 5), where the water type is estimated as oceanic OIB of Jerlov. Seven circles in Figure 8 a show that the 12 m threshold actually extends to in excess of 17 m.

Preprints (www.preprints.org) | NOT PEER-REVIEWED | Posted: 6 June 2017 doi:10.20944/preprints201706.0030.v1

The depth threshold used for the sea truth regression makes some sense, as the retrieved depth below the threshold is hardly affected by the uncertainty on Lsw_{PAN} (in the case of the PAN solution), unlike the deeper range above that threshold, which is most sensitive to a slight increase or decrease of this parameter. But the 4SM practitioner can -and must- investigate the water column corrected spectral reflectance result. Indeed, if Lsw_{PAN} is a bit too high, depths in the 17-30 m range will tend to be overestimated -more so as the bottom contrast gets close to extinction-, and the water column corrected reflectance shall be over-estimated accordingly; and *vice versa*. This shows in the display of a color composite of the water column corrected reflectance, and the practitioner must exercise caution and act accordingly by slightly adjusting the Lsw_{PAN} term. This discussion is related to the concept of a cut-off depth highlighted by the United Kingdom Hydrographic Office (UKHO) [22].

6.2. Path radiance La, and water volume reflectance Lw

The path radiance La needs not to be impeccable: what is needed is that the Soil Line be given the right spectral properties, *i.e.* ratios Lb_i/Lb_j. Negative radiances due to an approximate "atmospheric correction" can not be tolerated: this is a severe limit to the use of established atmospheric correction protocols which rely on atmospheric models.

In the 4SM approach, this is easily prevented, as the Lw term simply cannot be negative. Therefore, the water volume reflectance Lw is easily estimated as Lw=Lsw-La. But the practitioner needs to keep in mind the basics of water volume reflectance, and of its variation over the visible range as a function of spectral diffuse optical properties of the water *in situ*: the water volume reflectance term Lw is negligible over the NIR-red range, then increases smoothly through the orange-green range, then increases sharply over the blue range.

The depth retrieved over dark bottoms depends to a large extent on a correct estimation of the water volume reflectance term Lw, as may be verified by inspection of Figure 1a. This is an exclusive bonus of the 4SM approach over empirical approaches.

6.3. Spectral K, mid-waveband, and the far-green to red region

Spectral K is wavelength dependent in Jerlov's data. Each multispectral wide band has its own response curve; therefore, it is relevant to consider its effective -or operational- wavelength rather than its wavelength at mid-waveband. In view of all the simplifications of the RTE, this question might seem a third order technicality, but it is not for multispectral wide bands: for example, the Green wide band of LANDSAT-8 (530-590 nm) extends well over the steep increase in K between 550 and 600 nanometers signaled earlier. But Figure 6 shows that, even if discussing such technicality is relevant when using wide bands, it is not any more when using hyerspectral narrow bands: it has indeed become a fact that a good fit of the scatter of the BPL pixels in calibration diagrams, like illustrated in Figure 4, can only be achieved by decreasing operational spectral K in the far-green to far-red range of the solar spectrum for all pairs of bands. Therefore, it just happens that using the ratio K_{blue}/K_{green} observed in the image to interpolate K_{blue} and K_{green} at mid-wavelength then yields the right spectral K in m^{-1} over the whole visible range for use when operating the RTE. The end result is that CoefZ~=1 in the following

Preprints (www.preprints.org) | NOT PEER-REVIEWED | Posted: 6 June 2017 doi:10.20944/preprints201706.0030.v1

$$FinalSDBdepth = CoefZ \cdot SDBdepth - TideHeight \quad (14)$$

where CoefZ and TideHeight can only be estimated using sea truth data.

Therefore, there is a long way to go from Jerlov's "diffuse irradiance attenuation coefficient Kd" to operational K in the simplified RTE. Quite significantly, Jerlov [19] also commented: *"It should be borne in mind that, in the surface region 0-10m, the irradiance attenuation coefficient Kd for high solar elevation is close to the absorption coefficient a"* .

After all, one may consider that the path of bottom-reflected photons which reach the sensor's very narrow field of view is likely to have been very close to the vertical, both on its way down from the sea surface to the bottom, and on its way up from the bottom to the sea surface, with most other photons being scattered out of this near-vertical path. If this holds true, then one may consider that rewriting the simplified RTE for irradiances (1) into a new version for radiances, or digital numbers for that matter (2), now finds its justification. This aspect certainly warrants further academic investigation using a radiative transfer numerical model .

6.4. Homogeneous waters

The assumption of homogeneous waters may be considered a lost cause in many cases, even in atolls. But some variations in the optical properties can be accommodated in the the 4SM approach, to a limited extent: this is presented and discussed in Favoretto et al. [14].

6.5. Pan-sharpening, and the use of the panchromatic band

The panchromatic band may be used without pan-sharpening of the multispectral bands: for this it must be oversampled accordingly from 15 to 30 m GSD. But the panchromatic band may be used with pan-sharpening of the multispectral bands: for this various packages are available. Thanks to Fabio Favoretto (personal communication, 2016), our experience of using the Rstudio software package (https://www.rstudio.com/) for pan-sharpening works well, although the co-registration of the PAN band with other bands can be a problem. But, for a better control and for operational reasons, it is practical to include a pan-sharpening loop in the 4SM work flow. This is done as follows: after under-sampling the multispectral bands from 30 to 15 m GSD (a mere duplication of pixels), de-glinting (and before smoothing if required), let Ls_N be the radiance in band N at the center of a five pixels kernel: first a low-pass filter (LPF) is extracted as the average of panchromatic radiance in the kernel, then the following convolution is applied

$$Ls_N = Ls_N \cdot Ls_{PAN} / LPF \quad (15)$$

So, pixels which are brighter than their surrounding in the PAN band get a boost in the multispectral bands, and *vice versa*. This turns out to be very efficient and fast. Therefore, the SDB and water column corrected rasters are produced at the 15 m GSD.

Other empirical methods only use multispectral bands. This works as long as there is sufficient color separation: for example $K_{blue} < K_{green} < K_{red}$ as in clear oceanic waters: there is good color separation, and the ratio K_{blue}/K_{green} is much less than 1. But in Oceanic III or Coastal water types, there is hardly any color separation and the ratio K_{blue}/K_{green} gets very close to 1 or even worse: this

 doi:10.20944/preprints201706.0030.v1

precludes a reliable estimation of the model parameters in methods like Lyzenga's or Stumpf et al's. The PAN solution offers a valuable alternative, as there is always enough color separation, even with Coastal type waters.

6.6. Which inversion solution?

As exposed in section 2.2, several solutions can be operated for the inversion of the RTE. For example, a LANDSAT-8 pixel which exhibits significant bottom contrast Ls_4-Lsw_4 in the red band may usually be modeled using the Red solution, but the Green solution is also available. For areas modeled using the Red solution, the ratio $((LB_1+LB_2+LB_3)/3)/LB_4$ is to a large extent determined by the bottom contrast in the red band, and much less on the bottom contrast in other bands 1, 2 and 3. This becomes critical as the bottom contrast becomes nearly extinct, *i.e.* very close to its maximum optical depth K_{red}*$Zmax_{red}$: Lsw_{red} may be just a little too high and cause overestimation of the retrieved depth, and *vice versa*. This kind of uncertainty hardly affects the neighboring pixel if modeled by the Green solution at just a fraction of its maximum optical depth K_{green}*$Zmax_{green}$. As a result, an unsightly gap appears in the raster of retrieved depths along the frontier between areas modeled by either solution. Moreover, such gap tends to be either positive or negative and vary in intensity, as determined by slight local variations of the water's optical properties. This becomes even more of a nuisance when more wavebands, and therefore more solutions, are available, like when using a hyperspectral image. The end-user is not prepared to tolerate such gaps in a SDB product, which cast doubts on the overall approach.

In this regard, apart from accomodating a pan-sharpened image, a PAN solution offers the following distinct avantage: all shallow pixels are processed using the PAN solution, without any gap, over the whole shallow depth range.

6.7. Bottom typing

Water column corrected spectral bottom reflectances may be converted to calibrated reflectances, in the range 0-1, by use of the metadata provided with the LANDSAT-8 or WORLDVIEW-2 imagery. But, because of the depth residual, they are only a proxy to real bottom substrate reflectances. Nevertheless, they should prove useful in the case of time series monitoring.

The PAN solution is also beneficial for the purpose of bottom typing: first it frees the water column correction of the green band when computing the ratio $((LB_1+LB_2+LB_3)/3)/LB_{PAN}$; then all pixels are processed using the same solution over the whole depth range: this is a distinct bonus for bottom typing.

6.8. Transient heterogeneities, and combining depths

Transient heterogeneities cause very adverse artifacts, which cannot be avoided. Favoretto et al. [14] show how a time series of LANDSAT-8 images is used to produce a combined depth raster which is free of the transient encumbrances (clouds/shadows, seasonal variations, local blooms, heterogeneities of the atmosphere and water properties, boats and their wakes, *etc*): this raster then may be considered as a 15 m GSD DTM over the scene, which is tested against a quality sea truth dataset.

 doi:10.20944/preprints201706.0030.v1

6.9. Applicable to clear marine and fresh waters worldwide

It may easily be realized that the 4SM approach applies to all shallow waters, worldwide, as it does not use any existing information that is specific to the study case site. It was even applied on river sites, and on the ice shelf of Greenland.

6.10. Work flow and performance

In the past, we have done the calibration and processing of the 4SM approach, painstakingly using band maths in ERDAS and a spreadsheet, for student training purposes. Then we set out to write the 4SM code to cover the whole operation "on the fly", from (i) reading the raw 16-bits image, (ii) to de-glinting, and smart-smoothing or pan-sharpening, (iii) to extracting calibration data, (iv) to working out all parameters required to specify the simplified RTE for the scene under study, (v) then finally to processing the image, line by line, pixel wise, within hours of downloading the raw data. Then on occasion (vi) we proceed to combining depths from a time series of images to produce a complete and clean DTM of the shallow areas.

Acknowledgements

We thank Fabio Favoretto, PhD student, University of La Paz, Mexico, and Andy Waddington, of AWHydrographic, for reviewing this manuscript. Dr Stephane Maritorena offered us in 1994 a copy of his PhD manuscript thesis. The Service Hydrographique et Oceanographique de la Marine (SHOM) granted us in 1994 a bathymetric survey of the lagoon of Moorea, French Polynesia. Dr Erich Hochberg granted us in 1998 a copy of his Advanced Airborne Hyperspectral Imaging Sensors (AAHIS) image of Kaneohoe Bay, Hawaii. Professor Tommy Lindell, of Upsala University, Sweden, provided us with a copy of a LANDSAT TM image subset of Negril Shores, Jamaica, and with a small sea truth dataset; he co-presented the results in 1998 at the ERIM conference, San Diego [13]. The Institut Francais de Recherche pour l'Exploitation de la Mer (IFREMER) granted us in 1999 a non-exclusive license to pursue our work as a private project for our sole profit, and we used a number of SPOT 1 images of French Polynesia that belonged to IFREMER. Herb Ripley provided us in 1999-2005 with a copy of many very large CASI datasets collected by Hyperspectral Data International (HDI), along with occasional financial support, travel expenses, and with our first installation of LINUX in 1999 on a portable computer. Dr Gavin Manson provided us in 2001 with encouraging sea truth evidence using a CASI image of Prince Edward Island, Canada. Dr Serge Andrefouet, of the University of South Florida, granted us in 2002 copy of four IKONOS images, and promising sea truth evidence at Lee Stocking Island, Bahamas. Professor Andre Morel encouraged us in 2002 to publish our work. The Institut Geographique National (IGN) granted us a copy of a SPOT 5 pan-sharpened image of Sanaa, Yemen. Richard Chiles, of NPA-CGG, provided us in 2009-2015 many LANDSAT and WORLDVIEW2 images, under non-disclosure agreement, and paid us for part of the work done. Dr Ron Abileah, of JOMEGAK, granted us much encouragement and a copy of many WORLDVIEW2 images of Waimanalo Beach, Hawaii. Dr Gregory Miecznik, of Digital Globe Inc., provided us in 2012-2016 with many WV2 images, under non-disclosure agreement. Dr James Goodman, of Hyspeed Computing LLC, provided us in 2013 a copy of the CASI image of Heron Island, Great Barrier Reef, Australia, under license of the Center for Spatial Environmental Research at the University of Queensland. Dr Antoine Collin, of the Ecole Pratique des Hautes Etudes, provided us in 2014 with a copy of a pan-sharpened QUICKBIRD image of Shiraho Reef, Japan. Dr Emmanouil Oikonomou, of the Technological Institute of Athens, provided us in 2015 with a WORLDVIEW2 image of the Gulf of Laganas, Zakynthos Island, Greece.

Conflicts of interests: The institutions or individuals identified in the acknowledgements had no role in the design of the study; in the analyses, or interpretation of data; in the writing of the manuscript, and in the decision to publish the results. The author seeks commercial development of the 4SM approach.

Computer code and software: A basic version of the 4SM executable code is available, along with a tutorial using a subset of a SPOT 1 image of Tarawa atoll, Kiribati. It may be accessed at the following address: http://www.watercolumncorrection.com/4sm-tutorials.php. A demonstration is available for anyone to run on their own LINUX workstation, complete with 4SM executable code, image data and command line scripts; it uses a 17 bands CASI image of Heron Island, Great Barrier Reef, Australia. The output are rasters of de-glinted bands, SDB, rasters of water column corrected bands, bottom typing, and seatruth validation. This demonstration is available at http://www.watercolumncorrection.com/4sm-demonstration.php#download.Following this work, Dr James Goodman of Hyspeed Computing LLC, posted his comments on his website at https://hyspeedblog.wordpress.com/2014/01/14/bathymetry-and-water-column-correction-using-4sm-a-hyphoon-user-success-story/.

References

1. Lyzenga, D.R.; Passive remote sensing techniques for mapping water depth and bottom features. *Applied Optics* **1978**, *17*, 379–383.
2. Stumpf, R.P.; K. Holderied K.; M. Sinclair M. Determination of water depth with high-resolution satellite imagery over variable bottom types. *Limnology and Oceanography* **2003**, *48*, 547–556.
3. Pe'eri, S.; Azuike, C.; and Parrish, C. Satellite-Derived Bathymetry a Reconnaissance Tool for Hydrography. *Center for coastal ocean mapping*. **2013**.
4. International Hydrographic Organization, Intergovernmental Oceanographic Commission, The IHO-IOC GEBCO Cook Book, *IHO Publication B-11, IOC Manuals and Guides 63*, Monaco, France, Dec **2016**. 429 pp.
5. SPEAR Relative Water Depth, accessed on April 28th 2017 at https://www.harrisgeospatial.com/docs/SPEARRelativeWaterDepth.html
6. Camacho, M.A. Depth analysis of Midway atoll using QUICKBIRD multi-spectral imaging over variable substrates, *U.S. Naval Postgraduate School: Monterey, California*, **2006**.
7. Ehses, J.S.; Rooney, J.J. Depth derivation using multispectral WORLDVIEW-2 satellite imagery; *U.S. Dep. Commer., NOAA Tech. Memo*., NOAA-TM-NMFS-PIFSC-46. **2015**. 24p. doi: 10.7289, V5668B40.
8. Carmody, J.D. Deriving bathymetry from multispectral and hyperspectral imagery, *Thesis University of New South Wales*, 174 pages. Available online: http://unsworks.unsw.edu.au/fapi/datastream/unsworks:3188/SOURCE02?view=true (accessed on 27 April 2017), **2007**.
9. Hogrefe, K.R. Derivation of Near-shore Bathymetry from Multispectral Satellite Imagery used in a Coastal Terrain Model for the Topographic Analysis of Human Influence on Coral Reefs, Oregon State University, **2008**. ftp://ftp.soest.hawaii.edu/pibhmc/website/webdocs/documentation/Cookbook_042108.pdf
10. Lee, Z.; Carder K.L.; Mobley C.D.; Steward R.G., and Patch J.S.. *Hyperspectral remote sensing for shallow waters. 1. A semianalytical mode*. *Applied Optics* **1998**, *37*, 6329–6338.
11. Dekker, A.G.; Phinn, S.R.; Anstee, J.; Bissett, P., Brando, V.E. , Casey, B. , Fearns, P. , Hedley, J. , Klonowski, W. , Lee, Z.P.; Lynch, M.; Lyons, M.; Mobley, C.; Roelfsema, C. Intercomparison of shallow water bathymetry, hydro-optics, and benthos mapping techniques in Australian and Caribbean coastal environments. *Limnology and Oceanography* **2011**, *Methods 9*, 396–425.
12. Giardinoa, C.; Candiania, G.; Bresciania, M.; Lee, Z.P.; Gaglianoc, S.; Pepea, M. BOMBER: A tool for estimating water quality and bottom properties from remote sensing images. *Computers and Geosciences* **2012**, *45*, 313–318.

13. Morel, Y.; Lindell, T. Passive multispectral bathymetry mapping of Negril Shores, Jamaica. In *Fifth International Conference on Remote Sensing for Marine and Coastal Environments*; San Diego, California, **1998**.
14. Favoretto, F.; Morel, Y.; Waddington, A.; Lopez-Calderon J.; Blanco-Jarvio A. The Self-Calibrated Supervised Spectral Shallow-sea Modeler allows to produce low cost bathymetry with LANDSAT-8 in the Gulf of California, *in preparation* ***2017***.
15. Zoffoli, M.L.; Frouin, R.K.; Kampel, M. Water Column Correction for Coral Reef Studies by Remote Sensing. *Sensors* **2014**, 14, 16881-16931.
16. Philpot, W. Bathymetric mapping with passive multispectral imagery. *Applied Optics* **1989**, *28*, 1569–1578.
17. Maritorena, S.; Morel, A.; Gentilli, B. Diffuse reflectance of oceanic shallow waters: Influence of water depth and bottom albedo. *Limnology and Oceanography* **1994**, *37*, 1689–1703.
18. Maritorena ,S. Remote sensing of the water attenuation in coral reefs: a case study in French Polynesia. *International Journal of Remote Sensing* **1996**, *17*, 155–166.
19. Jerlov, N.G. Marine optics; *Elsevier Scientific Publishing Co*: Amsterdam, 1976.
20. Kirk, J.T.O. Light and photosynthesis in aquatic ecosystems; 2nd Edition.; *Cambridge University Press*: Cambridge, New York, Melbourne, **1994**.
21. Hedley, J.D.; Harborne, R.; Mumby, P.J. Simple and Robust Removal of Sun Glint for Mapping Shallow-water Benthos. *International Journal of Remote Sensing* **2005**, *26*, 2107–2112.
22. Talbot, A. Satellite Derived Bathymetry , *UKHO Report to NCWG1* – April **2015**, document CSPCWG11-08.7A- Satellite Bathymetry.pdf.
23. Morgan, W.; Harris, P. Developing Models and Analogs for Isolated Carbonate Platforms: *Holocene and Pleistocene Carbonates of Caicos Platform, British West Indies, AAPG SEPM Core Workshop 22.* **2008.**
24. Martin, J.; Eugenio, F.; Marcello, J.; Medina, A. Automatic Sun Glint Removal of Multispectral High-Resolution WORLDVIEW-2 Imagery for Retrieving Coastal Shallow Water Parameters. *Remote Sensing*. **2016**. 8-37.